Brillouin shift and linewidth measurement based on double-edge detection technology in seawater

K. Liang[1] · R. Zhang[1] · Q. Sun[2] · Y. Xu[1] · H. Wu[3] · P. Zhang[1] · B. Zhou[1]

Abstract

The seawater salinity and temperature of an ocean are key parameters required for environmental evaluation, with Raman and Brillouin scattering techniques offering a potentially accurate approach. A method for Brillouin scattering spectrum measurement based on a double-edge technique is proposed, and a retrieval model for simultaneously acquiring Brillouin shifts and linewidths is built. The accuracy of the proposed retrieval model is analyzed using simulations, and the results show that this double-edge technique provides good performance in terms of Brillouin scattering spectrum reconstitution and is a feasible method for simultaneous seawater temperature and salinity inversion.

1 Introduction

Raman and Brillouin scattering caused by the interaction between a laser and seawater molecules are related to both temperature and salinity, and remote sensing of these properties can be realized by detecting these two types of scattering spectrum [1, 2]. Because of the large frequency shift, wide spectrum, and relatively easy detection provided by Raman scattering, developments have been made in seawater temperature and salinity measurement using Raman scattering [3, 4]. However, from the perspective of scattering mechanisms, the Brillouin scattering cross-section is larger than that of Raman scattering, which results in a stronger echo energy intensity and deeper detection distance. In addition, the Brillouin scattering spectrum frequency shift is smaller and its distribution in the frequency domain is narrower than the Raman spectrum, while the corresponding background noise of a Brillouin scattering effective spectrum segment is lower, with a higher signal-to-noise ratio [5]. These advantages suggest that Brillouin scattering light detection and

ranging (lidar) is an important avenue for the development of seawater temperature and salinity measurement.

As a new detection technology, Brillouin lidar has already been used for ocean remote sensing. Through the extraction of chrematistic Brillouin spectrum parameters such as Brillouin shift and linewidth (full width at half maximum), the inversion of ocean environmental parameters, such as acoustic velocity, temperature, and salinity, and underwater target detection may be realized [6, 7].

In Brillouin lidar applications, the critical step is to accurately obtain the Brillouin spectrum. In general, a scanning Fabry–Perot (F–P) interferometer is used for high-precision Brillouin spectrum measurement [8]. However, an F–P scanning interferometer requires that the incident light be strictly collimated [9], which is difficult to achieve in a real environment. Furthermore, this type of scanning takes a certain amount of time [10], rendering it unable to provide real-time spectral measurement and limiting the practical application of Brillouin lidar.

To obtain Brillouin parameters in real time, Fry et al. employed the edge technique to measure Brillouin shift [11]. The basic idea of the edge technique is to local a frequent-dependent backscattering line on the steep edge of a transmission line of an optical filter so that a small frequency change can provide a large signal variation [12]. The iodine absorption cell was adopted as the edge filter, which had steep transmission edges located at the center of each Brillouin line with opposite slopes. The results indicated that edge technology was highly sensitive, although it was unable to provide the Brillouin linewidth, with the exception of the

✉ B. Zhou
  zhoubo@hust.edu.cn

1 School of Electronics and Information Engineering, Huazhong University of Science and Technology, Wuhan 430074, P.R. China

2 Beijing Institute of Space Mechanics and Electricity, Beijing 100076, China

3 The Third Department, China Ship Research and Development Academy, Wuhan 430074, China

Brillouin shift. Moreover, as the position of the absorption peak of the iodine molecule is fixed, the edge filter could not be adjusted.

To obtain a complete Brillouin spectrum, Liu et al. [13] later proposed a detection method based on F–P etalon and intensified charge-coupled device (ICCD). The Brillouin scattering echo passing through the F–P etalon is converted into interference fringes, which is then recorded by the ICCD. After signal processing, the Brillouin spectrum may be extracted from the interference signal of the ICCD. However, the limitation of the integral time of the ICCD means that the Brillouin scattering spectrum cannot be obtained quickly and continuously in this manner.

Considering the requirements of real-time and complex measurement of the aforementioned technologies, edge-detection technology provides the advantage of real-time measurement and is more suitable for practical applications. Nevertheless, the edge technique still requires two key improvements. First, a flexible edge filter should be developed, which suggests modifying the edge filter to adjust filtering position and bandwidth, and obtain a larger measurement range. T. Walther [14] designed an excited-state Faraday anomalous-dispersion optical filter (ESFADOF) to replace the I2/Br2 absorption filter. ESFADOF is a new type of edge filtering technique [15], which can control magnetic field intensity to find the appropriate edge filtering absorption function. In addition, the receiver of ESFADOF has a wide-range field of view, high noise-rejection ability, and short response time, which enhances the practicability of edge Brillouin lidar. Second, the measurement method of the edge technique must be improved. In current edge techniques, only the Brillouin shift may be obtained by detecting energy intensity, as opposed to the complete Brillouin spectrum, which means that a significant amount of important information such as the Brillouin linewidth is lost. The Brillouin linewidth is of great significance to the temperature, salinity, and attenuation coefficient of seawater [16]. Furthermore, as in the case of the Brillouin shift, the Brillouin linewidth also changes with temperature and salinity, which may both be related to energy intensity detection [17].

The purpose of this study is to improve the edge technique to measure the complete Brillouin scattering spectrum. In theory, the Brillouin scattering spectrum in a hydrodynamic regime, similar to that of water, can be expressed by the Lorenz function [18, 19], and this spectrum function is determined by the Brillouin shift and the Brillouin linewidth, implying that the Brillouin scattering spectrum may be obtained by measuring the two parameters simultaneously. Therefore, a method is proposed to obtain the Brillouin scattering spectrum using double-edge technology, as in applications in atmosphere wind measurement [20]. The purpose of the two edge filters here is to obtain

two Brillouin scattering spectral fragments with a high spectral resolution (HSR). When the environmental parameters of seawater (such as temperature and pressure) change, the energy intensity passing through these two filters will also vary. Hence, the Brillouin scattering spectrum of seawater may be restructured, and the temperature and salinity of seawater are measured by detecting the change of the energy intensity.

This method could expand the measurement functionality of the edge technique and enhance the application of Brillouin lidar in remote sensing of environmental factors such as ocean temperature and salinity. The rest of the paper is structured as follows. The measurement theory based on a double-edge filter is described in Sect. 2, and its optimization is described in Sect. 3. Section 4 details the retrieval model built based on this theory. Sections 5 and 6 provide an analysis of the model's performance and accuracy, respectively. Finally, Sect. 7 presents the conclusions of our study.

2 Theory

The edge technique was first proposed by Gelbwachs [21] in 1988 before Fry et al. [11] applied it to Brillouin shift measurement in ocean remote sensing.

For the edge filter, a steep slope is located along a Brillouin line. A small change in the Brillouin shift produces large changes in the transmitted light of the edge filter so that the Brillouin shift can be measured by detecting changes in the transmitted light. In general, the relative energy intensity is adopted in practical applications to reduce the influence of energy intensity instability on results. First, the bromine molecular absorption cell is used as a band-stop filter to remove the unshifted Rayleigh scattering light. The transmitted light is then split into two beams with equal energies by a 1:1 beam splitter. One beam is directly received by a detector with energy intensity S_1 as the reference energy intensity. The other beam passes through an iodine molecule absorption cell and is received by another detector, with energy intensity S_2. Energy intensity S_2 is related to the relative position between the Brillouin shift signal and the absorption line of the iodine molecule. $S(v_B) = S_1/S_2$ (v_B is the Brillouin shift of the Brillouin lines) provides a normalization ratio that may be used in Brillouin shift measurement.

When measuring the Brillouin shift using the edge technique, the energy intensity through the edge filter is only related to the Brillouin shift, assuming that the Brillouin linewidth has a constant value. A typical value of the Brillouin linewidth is 0.5 GHz [12], which corresponds to a seawater temperature of 25 ℃. In fact, Brillouin linewidth varies with changing temperature and salinity [22]. For seawater in the temperature range of 0−30 ℃ and salinity of 0−35 ‰, the Brillouin linewidth varies between 0.5 and

1.8 GHz. Therefore, the Brillouin linewidth affects the Brillouin shift measurement in the edge technique.

In theory, the Brillouin scattering spectrum of seawater is characterized by the Lorenz function [13, 23]:

$$f(v, v_B) = \frac{1}{\pi \Gamma_B} \left\{ \frac{1}{1 + [2(v - v_B)/\Gamma_B]^2} + \frac{1}{1 + [2(v + v_B)/\Gamma_B]^2} \right\}$$
(1)

where v_B is the Brillouin shift of the Brillouin lines, and Γ_B is the Brillouin linewidth. Equation (1) shows that two key parameters, v_B and Γ_B, are sufficient to describe the Brillouin scattering spectrum, and that it may be reconstructed if v_B and Γ_B are simultaneously known. In existing edge techniques, a single edge filter can be used to collect one characteristic signal, which may be used to obtain only

the Brillouin shift. To measure the Brillouin linewidth at the same time, two characteristic signals are required. Accordingly, the double-edge technique is proposed to simultaneously measure, v_B and Γ_B, as shown in Fig. 1.

Figure 1a shows the principle of the double-edge detection. As opposed to the single-edge technique, there are two edge filters in the range of the Brillouin scattering spectrum. Therefore, changes in temperature and salinity corresponding to the change in the Brillouin shift and linewidth will result in a change in the energy intensity passing through the two edge filters. If we assume that the two characteristic energies are independent variables, we can obtain the two variables, the Brillouin shift and linewidth measurement. Edge filters 1 (blue line) and 2 (red line) are located at the steep edges on different sides of the Brillouin peaks (green line) to extract two characteristic energies from the Brillouin scattering spectrum.

Fig. 1 The double-edge technique used in the Brillouin scattering spectrum. **a** Principle of the double-edge filtering technique. **b** Schematic of the experimental setup for the double-edge filtering method
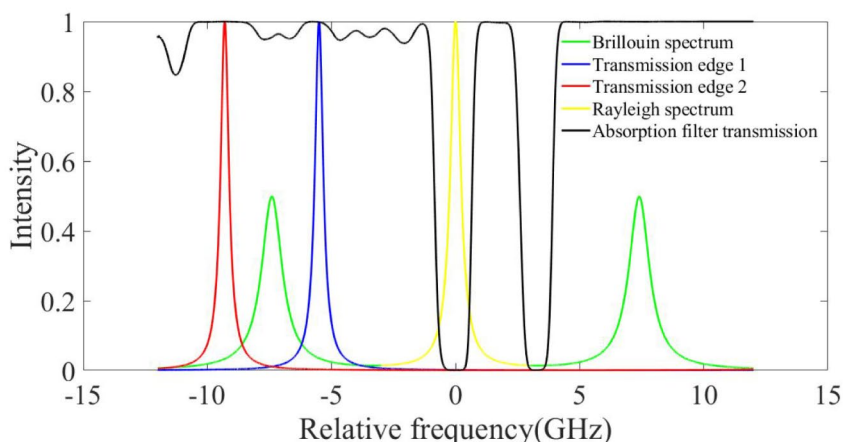
(a) Principle of the double-edge filtering technique.
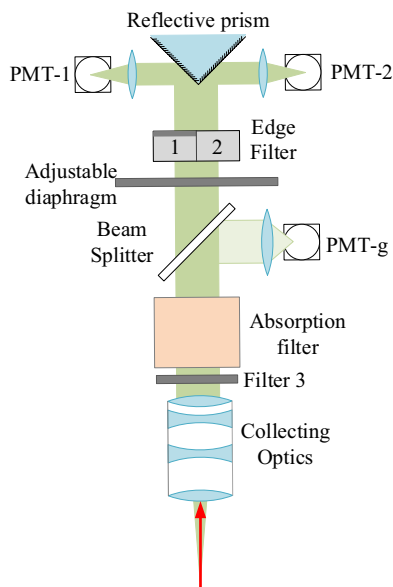
(b) Schematic of the experimental setup for the double-edge filtering method.

In theory, the energies passing through these two edge filters differ at a different Brillouin shift and linewidth, which can, in turn, be calculated using these two energies. To reduce the influence of Rayleigh scattering (yellow line), a band-stop filter is also required, as shown in Fig. 1a. This absorption filter (black line) is a band-stop filter that blocks the central Rayleigh line.

The receiver of a double-edge detection system is shown in Fig. 1b. Filter 3 is a narrow-band filter, which filters out background noise in the scattering spectrum that does not contain useful information. The returned scattering signal then passes through an absorption filter containing an absorption gas (iodine molecule absorption cell), which absorbs unshifted central Rayleigh scattering and transmits the Brillouin scattering energy intensity. The Brillouin scattered beam passes through a beam splitter that sends a fraction of the transmitted beam to the photon-counting detectors PMT-g to provide energy intensity I_g, and the remaining beam passes through edge filters 1 and 2. After passing through edge filter 1 and edge filter 2, the transmitted light is received by PMT-1 and PMT-2 with energies I_1 and I_2. Brillouin scattering spectrum I_B, after passing through the absorption filter, can be expressed as:

$$I_B(v_B, \Gamma_B) = \frac{1}{\pi} \cdot \left\{ \frac{\Gamma_B}{4(v - v_B)^2 + \Gamma_B^2} + \frac{\Gamma_B}{4(v + v_B)^2 + \Gamma_B^2} \right\} \tag{2}$$

where v_B is the Brillouin shift, and Γ_B is the Brillouin linewidth. The signal received by PMT-1 is:

$$I_1 = \int_{-\infty}^{+\infty} T_1(v - v_1, \Gamma_1) I_B(v_B, \Gamma_B) dv \tag{3}$$

and the signal received by PMT-2 is:

$$I_2 = \int_{-\infty}^{+\infty} T_2(v - v_2, \Gamma_2) I_B(v_B, \Gamma_B) dv \tag{4}$$

where $T_{i(i=1,2)}$ is the transmission function of the i th edge filter, and $v_{i(i=1,2)}$ and $\Gamma_{i(i=1,2)}$ are the central frequency and linewidth of the i th edge filter, respectively. When using F–P etalon as the edge filter, T_i can be expressed by the Airy function [24]:

$$T_i = \left[1 + \left(\frac{2FSR_i}{\pi \Gamma_i} \right)^2 \sin^2 \left(\frac{\pi}{FSR_i} v \right) \right]^{-1} \tag{5}$$

in which FSR_i is the free spectral range of the i th edge filter. The light I_g received by PMT-g is then calculated via:

$$I_g = \int_{-\infty}^{+\infty} f(v, v_B) dv \tag{6}$$

and the relative energies S_1 and S_2 can be written as:

$$S_1 = \frac{I_1}{I_g}, S_2 = \frac{I_2}{I_g}. \tag{7}$$

The Brillouin shift $v_B(S_1, S_2)$ and Brillouin linewidth $\Gamma_B(S_1, S_2)$ may be obtained using Eqs. (3), (4), (6), and (7), and the retrieval model for Brillouin shift and linewidth is established, as discussed in Sect. 4.

3 The optimization principle

Based on the aforementioned concepts, we may build a specific retrieval model for Brillouin shift and linewidth. To construct a retrieval model, we must optimize its parameters, and the influence of incident laser linewidth on the Brillouin scattering spectrum should be considered first. Assuming that the pulse spectrum of the employed laser is a Gaussian function with a linewidth less than 200 MHz (the incident laser wavelength is 532 nm), the convolution result with the Brillouin spectrum is shown in Fig. 2. The simulation results show that the pulse width of the laser has little effect on the Brillouin spectrum.

In the inversion of Brillouin shift and linewidth based on a double-edge filter, it is crucial to appropriately select the center frequency and linewidth of the two edge filters, which are directly related to retrieval model performance. To optimize these parameters and establish a retrieval model, we must consider the following three aspects: (1) Accuracy, the retrieval model should be able to accurately measure the Brillouin scattering spectrum and meet the accuracy requirements for remote sensing of ocean temperature and salinity; (2) Sensitivity: the energy intensity of the local narrow-band feature spectrum filtered by two edges should not be too weak to be effectively detected; (3) Large dynamic range: the energy intensity range under different conditions should
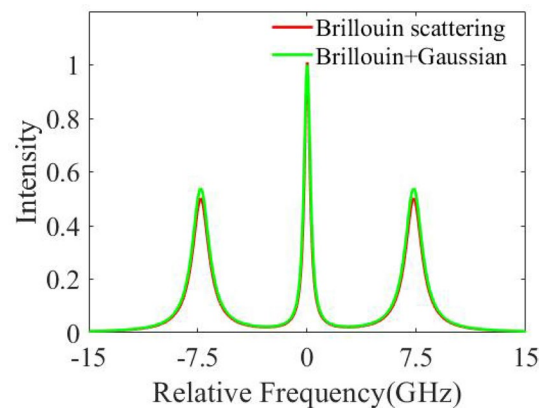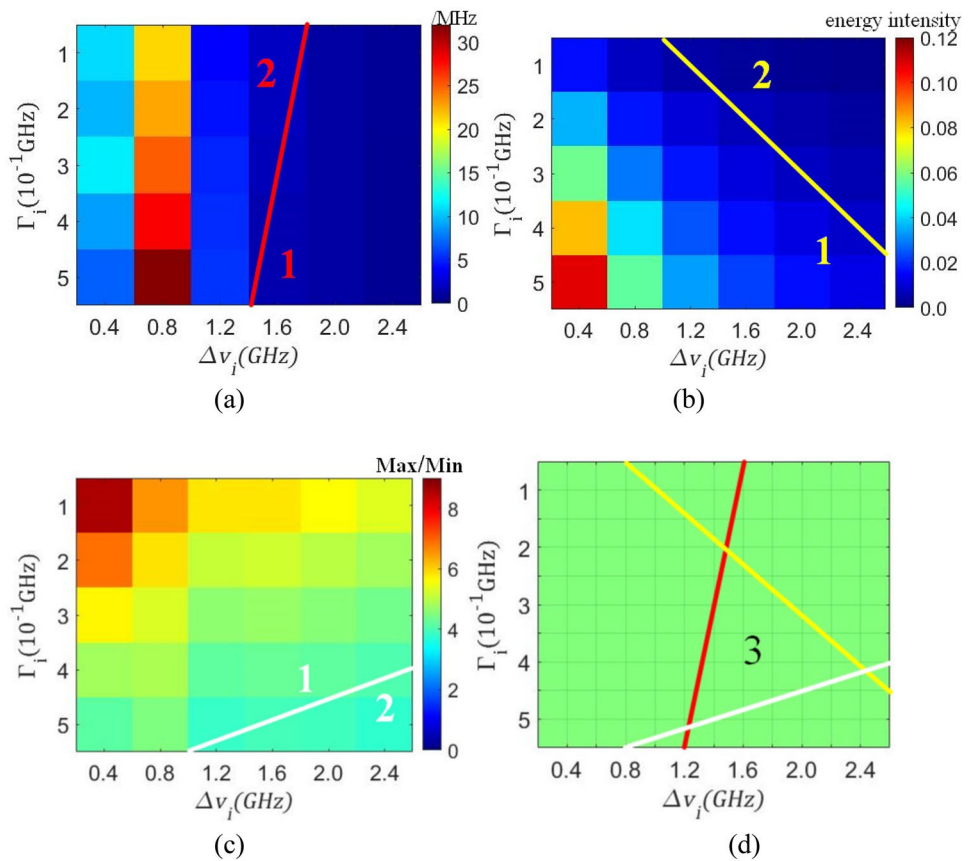

Fig. 2 Convolution results for laser pulse width and the Brillouin spectrum

Fig. 3 Optimization results for the double-edge filtering method. **a** The residual between the real data and the model, **b** the minimum energy intensity through the filter, **c** the range of the maximum to minimum energy intensity, and **d** a combination of the results of (**a**), (**b**), and (**c**)

(a)

(b)

(c)

(d)

be as large as possible, which could improve the robustness of the retrieval model.

Figure 3 shows the accuracy, sensitivity, and dynamic range of the system under different filter center frequency and linewidth parameters, where the horizontal axis shows half the relative frequency between the two edge filters. Considering that the Brillouin shift range is approximately 7.0−7.8 GHz, the center frequencies of these two edge filters are symmetrical at approximately 7.4 GHz. The vertical axis provides the linewidth of the filter.

We have calculated the inversion results of edge filters with different parameters, When the average error is 5 MHz, the inversion accuracy of Brillouin spectrum is 10 MHz, and the inversion errors of temperature and salinity are 1 ℃ and 2 ‰, respectively. Considering the current measurement range of most sensors, the minimum energy intensity should be greater than 0.01 to ensure a high signal-to-noise ratio of detection. According to the simulation results, when the dynamic range is greater than 4, it has high robustness. Figure 3a shows the average error between the calculated data and the data for the retrieval function. Considering limitations in accuracy, the average error should be less than 5 MHz, which is shown in zone 1 of Fig. 3a. When the relative energy intensity is greater than 0.01, it has better sensitivity, as shown in zone 1 in Fig. 3b. Dynamic range is expressed by the ratio of the

maximum energy intensity to the minimum energy intensity of the filter. It can be seen from Fig. 3(c) that when the filter parameter value is in zone 1, the dynamic range is greater than 4, which is what is required. Considering the above factors, the filter parameters are selected to be in zone 3 of Fig. 3d.

Finally, according to the above optimization principles, we conduct a more precise traversal search of zone 3, as shown in Fig. 3d, and select one group of optimal filter coefficients, as shown in Table 1, including the free spectral range (FSR) of each filter.

4 Retrieval model

After the filters are selected, the retrieval model is constructed using the following simulation steps. First, the relative energy intensities S_1 and S_2 are obtained under different

Table 1 Characteristics of filters A and B in the double-edge filtering method

	v_i/GHz	Γ_i/GHz	FSR /GHz
Filter A	5.5	0.4	25
Filter B	9.3	0.4	25

Brillouin shifts and linewidths, based on Eqs. (3), (4), (6), and (7). Tables 2 and 3 display the combinations of all possible Brillouin shift and linewidth values, without referring to the physical properties of water. In a real marine environment, it is impossible to obtain different Brillouin linewidths at a particular Brillouin shift. We adopt the method of simulation traversal to build the retrieval model, which contains the real data.

The values of relative energies S_1 and S_2 at a Brillouin shift v_B from 0.5 to 1.7 GHz and a Brillouin linewidth Γ_B from 7.0 to 7.8 GHz are shown in Tables 2 and 3, respectively. To obtain empirical equations for $v_B(S_1,S_2)$ and $\Gamma_B(S_1,S_2)$, we perform a least-squares fit to determine their functions, using the data fitting software:

$$\Gamma_B(S_1, S_2) = t_1 + t_2\ln(S_1) + t_3 S_2 + t_4\ln(S_1)^2 + t_5(S_2)^2 + t_6\ln(S_1)S_2 \\ + t_7\ln\left((S_1)^3\right) + t_8(S_2)^3 + t_9\ln(S_1)(S_2)^2 + t_{10}\ln(S_1)^2 S_2 \tag{9}$$

where r_i and t_i are the coefficients listed in Tables 4 and 5.

The values of the coefficients in Tables 4 and 5 are calculated by fitting 120 sets of data, where the coefficient of multiple determination $(R^2) = 0.99998$ and the residual sum of squares (Relative) $= 1.49055 \times 10^{-4}$ in Table 4. In Table 5, the coefficient of multiple determination $(R^2) = 0.99994$, and the residual sum of squares (Relative) $= 1.14762 \times 10^{-3}$.

Equations (8) and (9) form the retrieval model based on the double-edge technique, which indicates that the Brillouin shift and Brillouin linewidth can be inverted simultaneously.

$$v_B(S_1, S_2) = r_1 + r_2\ln(S_1) + r_3\ln(S_2) + r_4\ln(S_1)^2 + r_5\ln(S_2)^2 + r_6\ln(S_1)\ln(S_2) \\ + r_7\ln(S_1)^3 + r_8\ln(S_2)^3 + r_9\ln(S_1)\ln(S_2)^2 + r_{10}\ln(S_1)^2\ln(S_2) \tag{8}$$

Table 2 Calculated data for $S_1(v_B,\Gamma_B)(10^{-2})$ at different values of v_B and Γ_B

Γ_B(GHz)	v_B(GHz)								
	7.0	7.1	7.2	7.3	7.4	7.5	7.6	7.7	7.8
0.5	3.58	3.23	2.93	2.67	2.45	2.27	2.10	1.96	1.83
0.7	4.29	3.87	3.50	3.19	2.92	2.69	2.49	2.31	2.15
0.9	4.94	4.46	4.05	3.69	3.38	3.11	2.88	2.67	2.48
1.1	5.52	5.00	4.55	4.16	3.82	3.52	3.25	3.02	2.81
1.3	6.03	5.49	5.01	4.59	4.23	3.9	3.61	3.36	3.13
1.5	6.46	5.91	5.42	4.98	4.60	4.26	3.95	3.67	3.43
1.7	6.82	6.27	5.77	5.33	4.94	4.58	4.26	3.97	3.72

Table 3 Calculated data for $S_2(v_B,\Gamma_B)(10^{-2})$ at fixed values of v_B and Γ_B

Γ_B(GHz)	v_B(GHz)								
	7.0	7.1	7.2	7.3	7.4	7.5	7.6	7.7	7.8
0.5	1.64	1.76	1.91	2.07	2.26	2.48	2.74	3.04	3.4
0.7	2.00	2.16	2.34	2.55	2.78	3.05	3.37	3.73	4.16
0.9	2.36	2.55	2.76	3.00	3.27	3.58	3.94	4.36	4.85
1.1	2.71	2.92	3.15	3.42	3.72	4.07	4.47	4.92	5.44
1.3	3.03	3.26	3.52	3.81	4.14	4.51	4.93	5.41	5.96
1.5	3.34	3.59	3.87	4.18	4.52	4.91	5.35	5.85	6.41
1.7	3.63	3.89	4.18	4.51	4.86	5.27	5.71	6.21	6.78

Table 4 Coefficients of $v_B(S_1,S_2)$ for the double-edge method (Eq. (8))

Value	Standard error	Value	Standard error
$r_1 = 5.10357$	0.3843	$r_2 = -5.80701$	0.1885
$r_3 = 3.56109$	0.1750	$r_4 = -1.40797$	3.5268
$r_5 = 0.94482$	3.0184	$r_6 = -0.27057$	5.3537
$r_7 = -8.67401 \times 10^{-2}$	3.2680	$r_8 = 5.14992 \times 10^{-2}$	2.6116
$r_9 = 0.10638$	6.1181	$r_{10} = -0.15156$	6.5992

Table 5 Coefficients of $\Gamma_{\mathrm{B}}(S_1, S_2)$ for the double-edge method (Eq. (9))

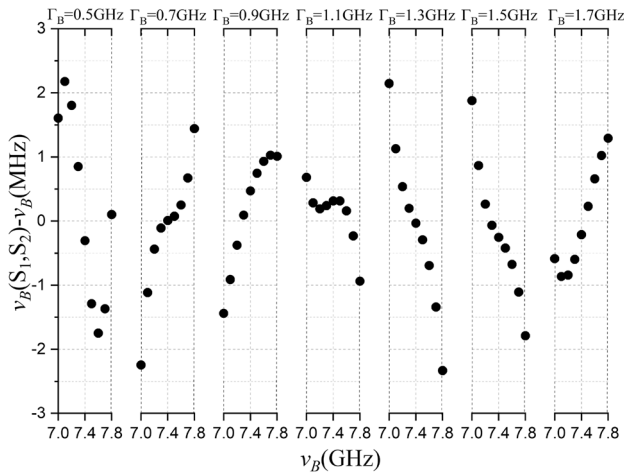| Value	Standard error	Value	Standard error
$t_1 = 1.15310$	0.4276	$t_2 = 2.18084$	0.3377
$t_3 = 282.22659$	6.8489	$t_4 = 0.97841$	0.0922
$t_5 = -162.50812$	46.7866	$t_6 = 124.06047$	3.5039
$t_7 = 0.13013$	8.8036	$t_8 = 2088.73843$	134.1312
$t_9 = 62.30442$	12.3828	$t_{10} = 15.46750$	0.4872

Fig. 4 Difference between the fitted Brillouin shift $v_{\mathrm{B}}(S_1, S_2)$ and theoretical Brillouin shift
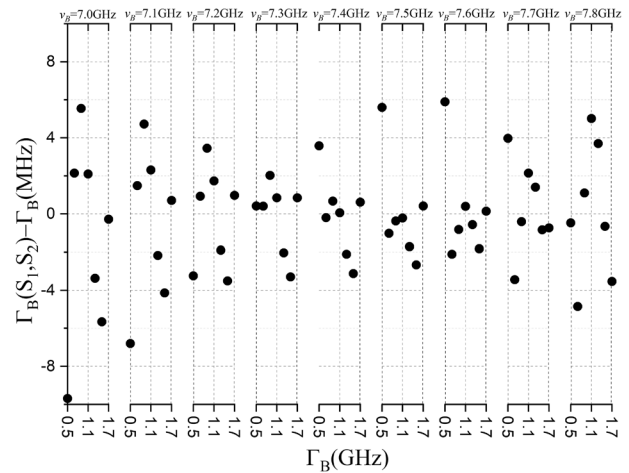

Fig. 5 Difference between the fitted Brillouin linewidth $\Gamma_{\mathrm{B}}(S_1, S_2)$ and theoretical Brillouin linewidth

5 Numerical analysis

To evaluate the performance of the retrieval model, the fitting error and dependence of the Brillouin shift and linewidth are analyzed. The differences between $v_{\mathrm{B}}(S_1, S_2)$ and $\Gamma_{\mathrm{B}}(S_1, S_2)$ from Eq. (8) and Eq. (9) and the corresponding values from Tables 2 and 3 are shown in Figs. 4 and 5.

Figures 4 and 5 show the error distributions of the Brillouin shift and Brillouin linewidth between the model and the values in Tables 2 and 3, respectively. The maximum error of the Brillouin shift obtained by the double-edge technique is 3 MHz, and the Brillouin linewidth error is within ± 6 MHz, with the exception of two individual points, which are still within ± 10 MHz. When using this model to measure the Brillouin shift and linewidth, these errors are within acceptable limits.

The dependence of the retrieval model on Brillouin shift and linewidth is also analyzed. In theory, Brillouin shift and linewidth are independent physical parameters, and in the proposed method they are determined only using the energy intensity ratios S_1 and S_2. To analyze the effect of S_1 and S_2 based on Eqs. (8) and (9), the changes in Brillouin shift caused by S_1 and S_2 can be expressed by:

$$\frac{\partial v_{\mathrm{B}}}{\partial S_1} = \frac{\partial v_{\mathrm{B}}(S_1, S_2)}{\partial S_1} + \frac{\partial v_{\mathrm{B}}(S_1, S_2)}{\partial S_2} \cdot \left[-\frac{\frac{\partial \Gamma_B(S_1, S_2)}{\partial S_1}}{\frac{\partial \Gamma_B(S_1, S_2)}{\partial S_2}} \right] \qquad (10)$$

and

$$\frac{\partial v_{\mathrm{B}}}{\partial S_2} = \frac{\partial v_{\mathrm{B}}(S_1, S_2)}{\partial S_2} + \frac{\partial v_{\mathrm{B}}(S_1, S_2)}{\partial S_1} \cdot \left[-\frac{\frac{\partial \Gamma_{\mathrm{B}}(S_1, S_2)}{\partial S_2}}{\frac{\partial \Gamma_{\mathrm{B}}(S_1, S_2)}{\partial S_1}} \right] \qquad (11)$$

Similarly, the sensitivity of S_1 and S_2 to Brillouin linewidth can be determined by:

$$\frac{\partial \Gamma_{\mathrm{B}}}{\partial S_1} = \frac{\partial \Gamma_{\mathrm{B}}(S_1, S_2)}{\partial S_1} + \frac{\partial \Gamma_{\mathrm{B}}(S_1, S_2)}{\partial S_2} \cdot \left[-\frac{\frac{\partial v_{\mathrm{B}}(S_1, S_2)}{\partial S_1}}{\frac{\partial v_{\mathrm{B}}(S_1, S_2)}{\partial S_2}} \right] \qquad (12)$$

and

$$\frac{\partial \Gamma_{\mathrm{B}}}{\partial S_2} = \frac{\partial \Gamma_{\mathrm{B}}(S_1, S_2)}{\partial S_2} + \frac{\partial \Gamma_{\mathrm{B}}(S_1, S_2)}{\partial S_1} \cdot \left[-\frac{\frac{\partial v_{\mathrm{B}}(S_1, S_2)}{\partial S_2}}{\frac{\partial v_{\mathrm{B}}(S_1, S_2)}{\partial S_1}} \right]. \qquad (13)$$

Table 6 Comparison between $\partial v_B/\partial S_1$ and $\partial v_B/\partial S_2$ for the double-edge method (S_1:1.83×10^{-2}—6.82×10^{-2}; S_2:1.64×10^{-2}—6.78×10^{-2})

Value (MHz/1%)	$(\partial V_B/\partial S_1)$	$(\partial V_B/\partial S_2)$
Maximum	0.0077	0.0042
Minimum	0.0018	0.0027
Average	0.0045	0.0034

Table 7 Comparison between $\partial \Gamma_B/\partial S_1$ and $\partial \Gamma_B/\partial S_2$ for the double-edge method (S_1:1.83×10^{-2}-6.82×10^{-2}; S_2:1.64×10^{-2}-6.78×10^{-2})

Value (MHz/1%)	$(\partial \Gamma_B/\partial S_1)$	$(\partial \Gamma_B/\partial S_2)$
Maximum	0.0071	0.0069
Minimum	0.0040	0.0027
Average	0.0052	0.0041

The sensitivity of the proposed model can be calculated using Eqs. (10)–(13). S_1 and S_2 are obtained through the photoelectric conversion of the PMT. According to the characteristics of the PMT, the noise of S_1 and S_2 should have a Poisson distribution in terms of its energy intensity. Therefore, the relative uncertainty of S_1 and S_2 is used to analyze the dependencies of the Brillouin shift and linewidth as a function of temperature and salinity. If the relative uncertainty in the intensity of S_1 and S_2 is approximately 1%, the maximum, minimum, and average values of $\partial v_B/\partial S_1$ and $\partial v_B/\partial S_1$ are obtained, as shown in Table 6.

These results indicate that both the range and the average value for $\partial v_B/\partial S_1$ are significantly greater than those of $\partial v_B/\partial S_2$, which proves that the impact of S_1 on the Brillouin shift is much larger than that of S_2.

We also make similar comparisons between $\partial \Gamma_B/\partial S_1$ and $\partial \Gamma_B/\partial S_2$, with the maximum, minimum, and average values of $\partial \Gamma_B/\partial S_1$ and $\partial \Gamma_B/\partial S_2$ provided in Table 7.

As shown in Table 7, there is no significant difference between $\partial \Gamma_B/\partial S_1$ and $\partial \Gamma_B/\partial S_2$, which proves that S_1 and S_2 have similar impacts on Brillouin linewidth.

6 Limitations of temperature and salinity measurement accuracy

Our ultimate goal is to measure seawater temperature and salinity, and so the uncertainties in the temperature and salinity values obtained using the proposed method must be further analyzed. Temperature and salinity can be obtained based on the Brillouin shift and linewidth [25],

$$T(v_B, \Gamma_B) = m_1 + m_2 \cdot v_B + \frac{m_3}{\Gamma_B} + m_4 \cdot v_B{}^2 + \frac{m_5}{\Gamma_B{}^2} + \frac{m_6 \cdot v_B}{\Gamma_B}$$
$$+ m_7 \cdot v_B{}^3 + \frac{m_8}{\Gamma_B{}^3} + \frac{m_9 \cdot v_B}{\Gamma_B{}^2} + \frac{m_{10} \cdot v_B{}^2}{\Gamma_B} \quad (14)$$

$$S(v_B, \Gamma_B) = k_1 + \frac{k_2}{v_B} + \frac{k_3}{v_B{}^2} + \frac{k_4}{v_B{}^3} + \frac{k_5}{v_B{}^4} + \frac{k_6}{v_B{}^5}$$
$$+ k_7 \cdot \ln\Gamma_B + k_8 \cdot \ln^2\Gamma_B + k_9 \cdot \ln^3\Gamma_B + k_{10} \cdot \ln^4\Gamma_B + k_{11} \cdot \ln^5\Gamma_B \quad (15)$$

where m_i and k_i are the coefficients, and can be found in [25]. Through error transfer analysis, we obtain the dependencies of temperature and salinity as a function of S_1 and S_2. The uncertainties in temperature and salinity depending on S_1 and S_2 are shown in Figs. 6 and 7.

In Figs. 6 and 7, the uncertainties in temperature and salinity depending on S_1 are less than 0.8 ℃ and 0.4 ‰, respectively; the uncertainties in temperature and salinity depending on S_2 are less than 0.3 ℃ and 1.4 ‰, respectively. The temperature uncertainty caused by S_1 is greater than that caused by S_2, though in terms of salinity, S_1 causes less uncertainty.

Some studies reported [25, 26] on the dependencies of temperature and salinity as a function of Brillouin shift and linewidth, proving that the impacts of Brillouin shift and linewidth on temperature are similar, but the impact of

Fig. 6 Temperature errors of the proposed double-edge method. **a** Temperature error of S_1, **b** temperature error of S_2
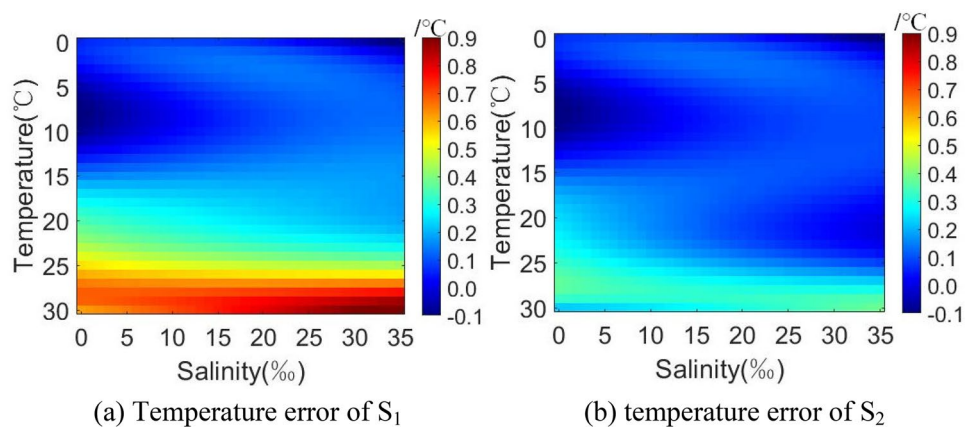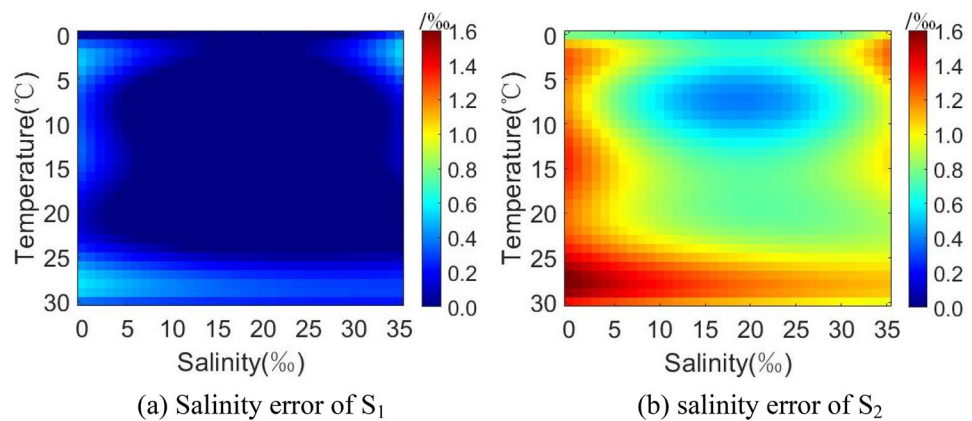

(a) Temperature error of S_1

(b) temperature error of S_2

Fig. 7 Salinity errors of the proposed double-edge method. **a** Salinity error of S_1, **b** salinity error of S_2

(a) Salinity error of S_1

(b) salinity error of S_2

Brillouin linewidth on salinity is much greater than that of Brillouin shift. Moreover, the higher the temperature, the greater the uncertainty in the temperature and salinity obtained using the Brillouin shift and linewidth. The results contained in Figs. 6 and 7 also indicate that when the seawater temperature is below 25 ℃, the uncertainty in the seawater temperature provided by the double-edge technique is 0.5 ℃, and the uncertainty in salinity is 1.2 ‰, which shows the high accuracy of the proposed method. For temperatures higher than 25 ℃, the uncertainties in temperature and salinity increase. The maximum temperature error is 0.9 ℃, and the maximum salinity error can reach 1.4 ‰. Therefore, the proposed double-edge method has a higher accuracy at low temperatures.

7 Conclusion

In this study, we propose a method for measuring the Brillouin scattering spectrum in seawater based on a double-edge technique. This technique employs edge filters on both sides of the Brillouin peaks to obtain two relative energy intensities. Based on these two relative intensities and corresponding functions, a retrieval model for Brillouin shift and linewidth is constructed. The error and sensitivity of the retrieval model are analyzed, with the results indicating that the errors in the Brillouin shift and linewidth of seawater are 3 MHz and 6 MHz, respectively. It is proved theoretically and experimentally that Brillouin scattering spectra of seawater can be obtained using the proposed double-edge technique.

In addition, the uncertainties in temperature and salinity depending on S_1 and S_2 are analyzed. At temperatures under 25 °C, temperature and salinity uncertainties are 0.5 ℃ and 1.2 ‰, respectively, which indicates that the double-edge technique is a feasible method for retrieving seawater temperature and salinity information. Based on the proposed method, our next work is to build the experimental setup and analyze performance.

References

1. J. Hirschberg, J. Byrne, A. Wouters, G. Boynton, Appl. Opt. **23**, 2624–2628 (1984)
2. C.P. Artlett, H.M. Pask, Proc. SPIE **8532**, 85320C (2012)
3. C.P. Artlett, H. Pask, Opt. Exp. **23**, 31844 (2015)
4. C.P. Artlett, H. Pask, Opt. Exp. **25**, 2840 (2017)
5. E.S. Fry, Y. Emery, X. Quan, J.W. Katz, Appl. Opt. **36**(27), 6887–6894 (1997)
6. J. Liu, J. Shi, X. He, S. Li, X. Chen, D. Liu, Opt. Commun **352**, 161–165 (2015)
7. A. Rudolf, T. Walther, Opt. Eng. **53**, 051407 (2014)
8. H. Sussner, R. Vacher, Appl. Opt. **18**, 3815–3818 (1979)
9. J. Xu, X. Ren, W. Gong, R. Dai, D. Liu, Appl. Opt. **42**, 6704–6709 (2003)
10. D. Liu, J. Xu, R. Li, R. Dai, W. Gong, Opt. Commun. **203**, 335–340 (2002)
11. Emery, Yves, E. S. Fry. Proc. SPIE 2963, Ocean Optics XIII, (1997)
12. R. Dai, W. Gong, J. Xu, X. Ren, D. Liu, Appl. Phys B **79**, 245–248 (2004)
13. J. Shi, M. Ouynag, W. Gong, S. Li, D. Liu, Appl. Phys. B **90**, 569–571 (2008)
14. K. Schorstein, A. Popescu, M. Göbel, T. Walther, Sensors **8**, 5820–5831 (2008)
15. A. Rudolf, T. Walther, Opt. Lett. **37**, 4477 (2012)
16. D. Liu, J. Shi, X. Chen, M. Ouyang, W. Gong, Front. Phys **5**, 82–106 (2010)
17. W. Gong, J. Shi, G. Li, D. Liu, J. Katz, E. Fry, Appl. Phys B **83**, 319–322 (2006)
18. I.L. Fabelinskii, *Molecular Scattering of Light* (Plenum, New York, 1968)
19. I.L. Fabelinskii, Prog. Opt. **37**, 97 (1997)
20. U. Marksteiner, C. Lemmerz, O. Lux, S. Rahm, A. Schäfler, Remote Sens. **10**, 2056 (2018)
21. J.A. Gelbwachs, IEEE J Quantum Elect **24**, 1266–1277 (1988)
22. E. Fry, J. Katz, D. Liu, T. Walther, J Mod. Opt. **49**, 411–418 (2002)
23. R. Mountain, J. Res. Natl. Bur. Stand. **70A**, 207–220 (1966)
24. G. Hernandez, Appl. Opt. **5**, 1745–1748 (1966)
25. K. Liang, Y. Ma, Y. Yu, J. Huang, H. Li, Opt. Eng. **51**(6), 066002 (2012)
26. Y. Yao, Q. Niu, K. Liang, Opt. Commun. **375**, 58–62 (2016)

Publisher's Note Springer Nature remains neutral with regard to jurisdictional claims in published maps and institutional affiliations.